Dynamic transition from insulating state to η-pairing state in a composite non-Hermitian system

X. M. Yang [1,3] and Z. Song [2,*]

[1] *School of Science, Chongqing University of Posts and Telecommunications, Chongqing 400065, China*

[2] *School of Physics, Nankai University, Tianjin 300071, China*

[3] *Institute for Advanced Sciences, Chongqing University of Posts and Telecommunications, Chongqing 400065, China*

(Received 20 December 2021; revised 10 April 2022; accepted 11 May 2022; published 23 May 2022)

The dynamics of Hermitian many-body quantum systems has long been a challenging subject due to the complexity induced by the particle-particle interactions. In contrast, this difficulty may be avoided in a well-designed non-Hermitian system. The exceptional point (EP) in a non-Hermitian system admits a peculiar dynamics: the final state being a particular eigenstate, coalescing state. In this work, we study the dynamic transition from a trivial insulating state to an η-pairing state in a composite non-Hermitian Hubbard system. The system consists of two subsystems, A and B, which are connected by unidirectional hoppings. We show that the dynamic transition from an insulating state to an η-pairing state occurs by the probability flow from A to B: the initial state is prepared as an insulating state of A, while B is left empty. The final state is an η-pairing state in B but empty in A. Analytical analyses and numerical simulations show that the speed of relaxation of the off-diagonal long-range order pair state depends on the order of the EP, which is determined by the number of pairs and the fidelity of the scheme is immune to the irregularity of the lattice.

DOI: 10.1103/PhysRevB.105.195132

I. INTRODUCTION

Experimental advances in atomic physics, quantum optics, and nanoscience have made it possible to realize artificial systems. It is fascinating that some of them are described by the Hubbard model [1] to a high degree of accuracy [2,3]. Then one can experimentally realize and simulate the physics of the model. The Hubbard model is a simple lattice model with particle interactions and has been intensely investigated in various contexts ranging from quantum phase transition [4,5] to high temperature superconductivity [6–8]. Direct simulations of such a simple model is not only helpful to solve important problems in condensed matter physics, but also to the engineering design of quantum devices. Importantly, the availability of experimental controllable Hubbard systems provides an unprecedented opportunity to explore the nonequilibrium dynamics in interacting many-body systems.

Very recently, it has been demonstrated that nonequilibrium many-body dynamics provides an alternative way to access a new exotic quantum state with energy far from the ground state [9–16]. It makes it possible to design interacting many-body systems that can be used to prepare some desirable many-body quantum states in principle. Unlike traditional protocols based on a cooling down mechanism, quench dynamics has a wide range of potential applications, since it provides many ways to take a system out of equilibrium, such as applying a driving field or pumping energy or particles in the system through external reservoirs [17–19]. In the recent work Ref. [20], a scheme has been proposed to realize quantum mold casting, i.e., engineering a target quantum state on demand by the time evolution of a trivial initial state. The underlying mechanism is pumping fermions from a trivial subsystem to the one with topological quantum phase. In this work, we extended this approach to interacting many-body systems.

In general, the time dynamics of Hermitian many-body quantum systems has long been an elusive subject, due to the complexity induced by the particle-particle interactions. The main obstacle is that the evolved state is not easily predictable in most cases. Nevertheless, this difficulty may be avoided in a well-designed non-Hermitian system, since the exceptional point (EP) in a non-Hermitian system admits a peculiar dynamics: the final state being a particular eigenstate, coalescing state [21–25]. The key point is the exceptional dynamics, which allows particles pumping from the source subsystem to the central subsystem, realizing the dynamical preparation of many-body quantum states. In the present work, we study the dynamic transition from a trivial insulating state to an η-pairing state in a composite non-Hermitian Hubbard system. The system consists of two subsystems, A and B, which is connected by unidirectional hoppings. Based on the performance of the system at EP, a scheme that produces a nonequilibrium steady superconductinglike state is proposed. Specifically, for an initial state with fully filled in A, but empty in B, unidirectional hoppings can drive it to the resonant coalescing state that favors superconductivity manifested by the off-diagonal long-range order (ODLRO). Such a dynamical scheme can be realized no matter what the shapes of the two sublattices of the composite system. Therefore, our finding is distinct from the previous investigations [13–15], and provides a quantum casting mechanism for generating superconductivity through nonequilibrium dynamics. On the other hand, the remarkable observation from our work can

*songtc@nankai.edu.cn

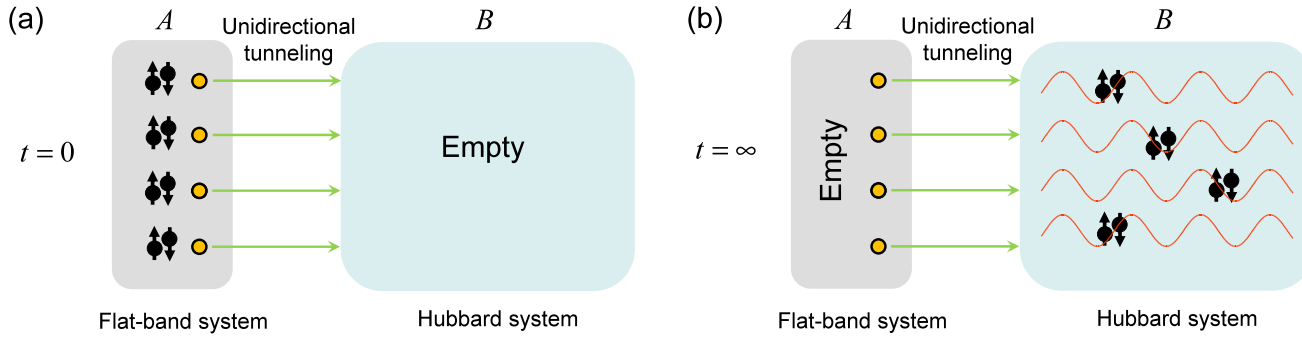

FIG. 1. The system consists of two subsystems, A and B, which are connected by unidirectional hoppings. A is an interaction-free system with trivial flat band, while B is a Hubbard system, which supports η-pairing eigenstates. At $t = 0$, A is fully filled as a trivial insulating state and B is empty. When the unidirectional hoppings switch on, the probability flows from A to B. After a long time, subsystem A becomes empty and subsystem B is in an η-pairing state, a condensation of bound pairs.

trigger further studies of both fundamental aspects and potential applications of composite non-Hermitian many-body systems.

The rest of this paper is organized as follows. In Sec. II, we present the model and its properties relating to η operators, or η symmetry. Section III is devoted to a doublon effective Hamiltonian which captures the physics in a fixed energy shell. In Sec. IV, we present the Jordan form with high-order EP based on the effective Hamiltonian. In Sec. V, numerical simulations are performed to estimate the efficiency of our scheme in various values of correlation strengths. Section VI concludes this paper. Some nonessential details of our calculation are placed in Appendices.

II. MODEL AND η OPERATORS

We consider a composite non-Hermitian system, described by the Hamiltonian

$$H = H_{\rm A} + H_{\rm B} + H_{\rm AB}, \tag{1}$$

with Hermitian terms

$$H_{\rm A} = \frac{U}{2}\sum_{i=1}^{N_a}(a_{i,\uparrow}^\dagger a_{i,\uparrow} + a_{i,\downarrow}^\dagger a_{i,\downarrow}),$$

$$H_{\rm B} = \sum_{\sigma=\uparrow,\downarrow}\sum_{i,j=1}^{N_b}(J_{ij}b_{i,\sigma}^\dagger b_{j,\sigma} + {\rm H.c.}) + U\sum_{i=1}^{N_b} b_{i,\uparrow}^\dagger b_{i,\downarrow}^\dagger b_{i,\downarrow}b_{i,\uparrow}, \tag{2}$$

and the non-Hermitian term

$$H_{\rm AB} = \sum_{\sigma=\uparrow,\downarrow}\sum_{i=1}^{N_a}\sum_{j=1}^{N_b}\kappa_{ij}b_{j,\sigma}^\dagger a_{i,\sigma}, \tag{3}$$

where $a_{i,\sigma}$ and $b_{j,\sigma}$ are fermion operators with spin-$\frac{1}{2}$ polarization $\sigma = \uparrow, \downarrow$ in lattices N_a and N_b, respectively. The parameters J_{ij} $(i, j \in N_b, i \neq j)$ and κ_{ij} $(i \in N_a, j \in N_b)$ are intra- and intercluster hopping strengths, and taken to be real in this paper. Here both $H_{\rm A}$ and $H_{\rm B}$ are Hermitian, describing the source system and the central system, respectively. $H_{\rm A}$ is an interaction-free system with trivial full flat band, while $H_{\rm B}$ is a standard Hubbard model, which is restricted to be the bipartite lattice. In particular, the key features of the setup are as follows: (i) $H_{\rm AB}$ is non-Hermitian, representing unidirectional tunnelings between two subsystems $H_{\rm A}$ and $H_{\rm B}$. (ii) The on-site potential of a pair of fermions in $H_{\rm A}$ is identical to the on-site repulsion in $H_{\rm B}$, but a little difference will not affect the scheme since the EP dynamics can be extended to the near-EP dynamics [20]. The schematic of the system is presented in Fig. 1.

We define two η operators for two subsystems:

$$\eta_{\rm A}^\dagger = \sum_{i=1}^{N_a}\eta_{{\rm A},i}^\dagger = \sum_{i=1}^{N_a}\alpha_i a_{i,\uparrow}^\dagger a_{i,\downarrow}^\dagger, \tag{4}$$

$$\eta_{\rm B}^\dagger = \sum_{i=1}^{N_b}\eta_{{\rm B},i}^\dagger = \sum_{i=1}^{N_b}\beta_i b_{i,\uparrow}^\dagger b_{i,\downarrow}^\dagger, \tag{5}$$

where $\alpha_i = \pm 1$ can be taken arbitrarily, since there are no tunnelings between any two sites in the subsystem A, while $\beta_i = 1$ and -1, for the different sublattice i belongs to in the bipartite lattice B. It can be shown that both operators satisfy

$$[H_{\rm A}, \eta_{\rm A}^\dagger] = U\eta_{\rm A}^\dagger, [H_{\rm B}, \eta_{\rm B}^\dagger] = U\eta_{\rm B}^\dagger, \tag{6}$$

which can be utilized to construct the eigenstates of $H_{\rm A}$, $H_{\rm B}$, $H_{\rm A} + H_{\rm B}$,

$$|n\rangle_{\rm A} = \frac{1}{\sqrt{\Omega_{{\rm A},n}}}(\eta_{\rm A}^\dagger)^n|{\rm Vac}\rangle, \tag{7}$$

$$|m\rangle_{\rm B} = \frac{1}{\sqrt{\Omega_{{\rm B},m}}}(\eta_{\rm B}^\dagger)^m|{\rm Vac}\rangle, \tag{8}$$

where $\Omega_{{\rm A},n} = (n!)^2 C_{N_a}^n$ and $\Omega_{{\rm B},m} = (m!)^2 C_{N_b}^m$ are normalization factors.

$$H_{\rm A}|n\rangle_{\rm A} = nU|n\rangle_{\rm A}, \quad H_{\rm B}|m\rangle_{\rm B} = mU|m\rangle_{\rm B} \tag{9}$$

and

$$(H_{\rm A} + H_{\rm B})|n\rangle_{\rm A}|m\rangle_{\rm B} = (n+m)U|n\rangle_{\rm A}|m\rangle_{\rm B}. \tag{10}$$

We can find that the set of eigenstates $|n\rangle_{\rm A}|m\rangle_{\rm B}$ are degenerate for fixed $m + n$.

In general, an η-pairing state can be regarded as the condensation of bound pair fermions as hard-core boson. However, state $|n\rangle_{\rm A}$ is trivial since it is just one of multifold degenerate eigenstates. In addition, fully filled state $|N_a\rangle_{\rm A}$ and $|N_b\rangle_{\rm B}$ are insulating states and can be easily prepared. The

desirable states are $|N_a\rangle_{\rm A}|m\rangle_{\rm B}$ and $|0\rangle_{\rm A}|m\rangle_{\rm B}$ with $1 < m < N_b$, since both states possess ODLRO in subsystem B.

III. DOUBLON EFFECTIVE HAMILTONIAN

Like most interacting many-body systems, the exact solution of H is rare although states $|n\rangle_{\rm A}|m\rangle_{\rm B}$ are eigenstates of $H_{\rm A}+H_{\rm B}$. In order to capture the physics of our scheme, we will consider the problem in an energy shell. In the Hermitian system, one can employ the perturbation method to get the effective Hamiltonian. However, the corresponding theory has not been well established for the non-Hermitian system, especially for the unidirectional hopping perturbation. In the two Appendices, we have illustrated how to obtain the effective Hamiltonian of a non-Hermitian system from two perspectives. Appendix A provides an accurate effective Hamiltonian of a two-site non-Hermitian system from the time evolution operator, while Appendix B obtains the effective Hamiltonian of an arbitrary-sized non-Hermitian system for large U limit from parameters approaching the EP.

In this work, our aim is the dynamics for a special initial state, with subsystem A being fully occupied. It motivates us to consider pure doublon states in subsystem B, which has the same energy shell as that of the initial state. We take the parameter κ_{ij} as a constant $\kappa\delta_{ij}$ for simplicity. For a subspace spanned by a set of basis of the doublon state $\{|\Psi_{\rm D}^{\rm B}(n)\rangle, n\in[1,N_b]\}$, the effective Hamiltonian can be written as

$$H_{\rm B}^{\rm eff}=\sum_{i,j=1}^{N_b}\frac{-4J_{ij}^2}{U}\left(\boldsymbol{\eta}_{{\rm B},i}\cdot\boldsymbol{\eta}_{{\rm B},j}-\frac{1}{4}\right)+U\sum_{i=1}^{N_b}\left(\frac{1}{2}+\eta_{{\rm B},i}^{z}\right), \tag{11}$$

in the case of $U\gg|J_{ij}|$. Here a doublon state is

$$|\Psi_{\rm D}^{\rm B}(n)\rangle=b_{j_1,\uparrow}^{\dagger}b_{j_1,\downarrow}^{\dagger}b_{j_2,\uparrow}^{\dagger}b_{j_2,\downarrow}^{\dagger}\ldots b_{j_n,\uparrow}^{\dagger}b_{j_n,\downarrow}^{\dagger}|{\rm Vac}\rangle, \tag{12}$$

with $j_n\in[1,N_b]$, and the pseudospin operator is defined as $\boldsymbol{\eta}_{{\rm B},j}=(\eta_{{\rm B},j}^{+}/2+\eta_{{\rm B},j}^{-}/2,\eta_{{\rm B},j}^{+}/2i-\eta_{{\rm B},j}^{-}/2i,\eta_{{\rm B},j}^{z})$ with $\eta_{{\rm B},j}^{+}=\beta_j b_{j,\uparrow}^{\dagger}b_{j,\downarrow}^{\dagger}$ and $\eta_{{\rm B},j}^{z}=(n_{{\rm B},j,\uparrow}+n_{{\rm B},j,\downarrow}-1)/2$. Similarly, for a subspace spanned by a set of basis of the doublon state $\{|\Psi_{\rm D}^{\rm A}(n)\rangle, n\in[1,N_a]\}$, which means n lattice sites in subsystem A are occupied by two particles with opposite spin orientation, the effective Hamiltonian can be written as

$$H_{\rm A}^{\rm eff}=U\sum_{i=1}^{N_a}\left(\frac{1}{2}+\eta_{{\rm A},i}^{z}\right), \tag{13}$$

and corresponding operators obey the Lie algebra, i.e., $[\eta_{{\rm A},i}^{+},\eta_{{\rm A},j}^{-}]=2\eta_{{\rm A},j}^{z}\delta_{ij}$ and $[\eta_{{\rm A},i}^{z},\eta_{{\rm A},j}^{\pm}]=\pm\eta_{{\rm A},j}^{\pm}\delta_{ij}$.

Now, we turns to establish the effective Hamiltonian of the non-Hermitian term $H_{\rm AB}$. Unlike the Hermitian term, there is no unquestioned perturbation theory for the non-Hermitian perturbation, especially near the EP. In this work, we present the effective Hamiltonian $H_{\rm AB}^{\rm eff}$ from two perspectives. In the Appendices, we show that, for the given initial state with full filling A lattice and empty B lattice, the dynamics obeys the effective Hamiltonian

$$H^{\rm eff}=H_{\rm A}^{\rm eff}+H_{\rm B}^{\rm eff}+H_{\rm AB}^{\rm eff} \tag{14}$$

with

$$H_{\rm AB}^{\rm eff}=\frac{4\kappa^2}{U}\sum_i\eta_{{\rm A},i}^{-}\eta_{{\rm B},i}^{+}, \tag{15}$$

where

$$\eta_{{\rm A},i}^{-}=(-1)^i a_{i,\downarrow}a_{i,\uparrow},\qquad \eta_{{\rm B},i}^{+}=(-1)^i b_{i,\uparrow}^{\dagger}b_{i,\downarrow}^{\dagger}. \tag{16}$$

It is clear that $H_{\rm AB}^{\rm eff}$ is still a non-Hermitian term which describes a unidirectional hopping of a doublon or magnon from the point of view of spin wave.

Defining a total pseudospin operator

$$\eta^{z}=\sum_{i=1}^{N_a}\eta_{{\rm A},i}^{z}+\sum_{j=1}^{N_b}\eta_{{\rm B},j}^{z}, \tag{17}$$

we note that η^z is conservative for the Hamiltonian $H^{\rm eff}$ due to the commutation relation

$$[\eta^{z},H^{\rm eff}]=0, \tag{18}$$

which ensures that the Hilbert space of $H^{\rm eff}$ can be decomposed into many invariant subspaces labeled by the eigenvalues of η^z, i.e., $2\eta^z=-N_a-N_b$, $-N_a-N_b+1$,..., N_a+N_b-1, N_a+N_b. In this work, we only focus on the subspace with $\eta^z=(N_a-N_b)/2$ ($N_a<N_b$), which contains the initial state with fully filling A sublattices and empty B sublattices, i.e., $\prod_{i=1}^{N_a}a_{i,\uparrow}^{\dagger}a_{i,\downarrow}^{\dagger}|{\rm Vac}\rangle$.

IV. JORDAN FORM WITH HIGH-ORDER EP

In the above, we know that there are many degenerate eigenstates for $H_{\rm A}+H_{\rm B}$, which may become coalescing states when the proper non-Hermitian term is added [26]. For non-Hermitian operators, when the EP appears, there are eigenstates that coalesce into one state, leading to an incomplete Hilbert space [21–24]. Mathematically, it relates to the Jordan block form in the matrix [27–30]. Remarkably, the peculiar features around the EP have sparked tremendous attention to the classical and quantum photonic systems. The corresponding intriguing dynamical phenomena include asymmetric mode switching [31], topological energy transfer [32], robust wireless power transfer [33], and enhanced sensitivity [34–37] depending on their EP degeneracies. Many works have been devoted to the formation of the EP and corresponding topological characterization in both theoretical and experimental aspects [38–40]. In this work, we employ the EP dynamics to prepare states with ODLRO. We start with the Jordan form with high-order EP.

Considering two degenerate eigenstates $|A\rangle$ and $|B\rangle$ of the Hermitian Hamiltonian $H_{\rm A}+H_{\rm B}$, where

$$|A\rangle=|N_a\rangle_{\rm A}|0\rangle_{\rm B}=\frac{1}{\sqrt{\Omega_{{\rm A},N_a}}}(\eta_{\rm A}^{\dagger})^{N_a}|{\rm Vac}\rangle, \tag{19}$$

$$|B\rangle=|0\rangle_{\rm A}|N_a\rangle_{\rm B}=\frac{1}{\sqrt{\Omega_{{\rm B},N_a}}}(\eta_{\rm B}^{\dagger})^{N_a}|{\rm Vac}\rangle, \tag{20}$$

we have

$$H|B\rangle=N_aU|B\rangle,\quad H^{\dagger}|A\rangle=N_aU|A\rangle, \tag{21}$$

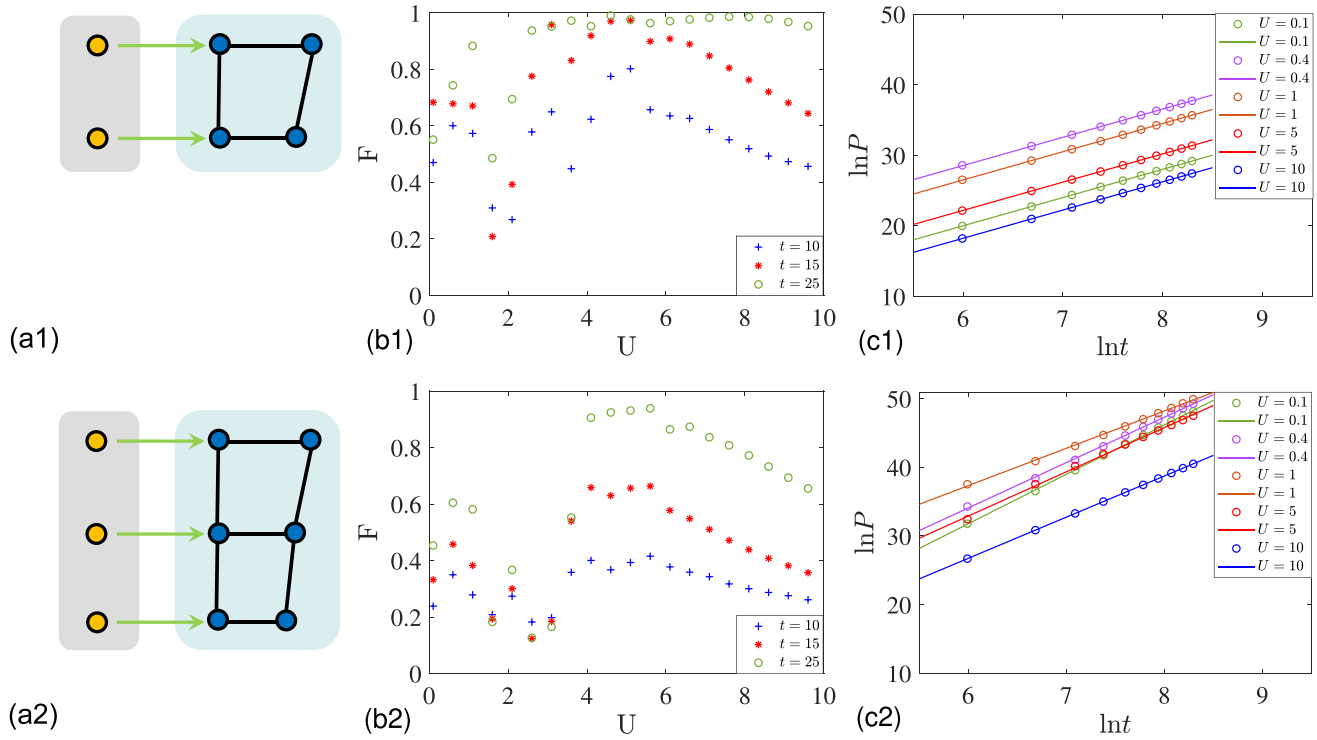

FIG. 2. Schematic illustration of (a1) a six site composite non-Hermitian system with four filled particles and (a2) a nine site composite non-Hermitian system with six filled particles concerning the following numerical simulations. The parameters are $\kappa = 1$, (a1)–(c1) $N_a = 2$, $N_b = 4$, $J_{ij} = 0.75, 1.17, 0.68, 1.02$; (a2)–(c2) $N_a = 3$, $N_b = 6$, $J_{ij} = 0.75, 1.17, 0.68, 1.02, 0.87, 0.61, 0.72$. (b1) and (b2) are plots of fidelity $F(t)$ defined in Eq. (37). Three typical values of t are taken and indicated in the panels. The numerical data oscillate at small U values and the optimal U occurs around $U = 5$. (c1) and (c2) show the scaling law of probability P defined in Eq. (36) as a function of t for different values of U. Different colored dots represent the numerical data, which are fitted by different colored solid lines (c1) $\ln P = 3.99 \ln t - 3.96$, $\ln P = 3.97 \ln t + 4.77$, $\ln P = 3.98 \ln t + 2.67$, $\ln P = 3.99 \ln t - 1.81$, $\ln P = 4.00 \ln t - 5.76$ and (c2) $\ln P = 7.20 \ln t - 11.40$, $\ln P = 6.61 \ln t - 5.56$, $\ln P = 5.44 \ln t + 4.66$, $\ln P = 6.45 \ln t - 5.80$, $\ln P = 6.00 \ln t - 9.26$ from $U = 0.1$ to $U = 10$, respectively.

due to the facts

$$H_{\mathrm{AB}}|0\rangle_{\mathrm{A}}|N_a\rangle_{\mathrm{B}} = 0, \quad (H_{\mathrm{AB}})^{\dagger}|N_a\rangle_{\mathrm{A}}|0\rangle_{\mathrm{B}} = 0. \tag{22}$$

It means that two states $|A\rangle$ and $|B\rangle$ are mutually biorthogonal conjugate and $\langle A|B\rangle$ is the biorthogonal norm of them. On the other hand, we have

$$\langle A|B\rangle = 0. \tag{23}$$

The vanishing norm indicates that state $|B\rangle$ ($|A\rangle$) is the coalescing state of H ($H^{\dagger}$), or Hamiltonians H and $H^{\dagger}$ get an EP.

However, it is a little hard to determine the corresponding Jordan block form and the order of the EP. In the following, we estimate the order in large U limit. At first, the above analysis for two states $|A\rangle$ and $|B\rangle$ is applicable for the effective Hamiltonian H^{eff}. This means that there is an EP in the invariant subspace with $\eta^z = (N_a - N_b)/2$, and dimension $C^{N_a}_{N_a+N_b}$. The order of such an EP is determined by the corresponding Jordan block. Second, when we consider a complete set of degenerate eigenstates of the Hermitian Hamiltonian $H_{\mathrm{A}} + H_{\mathrm{B}}$ in this subspace, which are denoted as $\{|n\rangle_{\mathrm{A}}|m\rangle_{\mathrm{B}}\}$ ($n \in [0, N_a]$, $N_a \leqslant N_b$) with fixed $m + n = N_a$, the effective Hamiltonian can be expressed as an $(N_a + 1) \times (N_a + 1)$ matrix M with nonzero matrix elements

$$\begin{aligned}(M)_{N_a+1-n,N_a-n} &= \langle N_a - n|_{\mathrm{B}}\langle n|_{\mathrm{A}} H^{\mathrm{eff}}|n+1\rangle_{\mathrm{A}}|N_a - n - 1\rangle_{\mathrm{B}} \\ &= \frac{4\kappa^2}{U}\frac{N_a - n}{N_b}\sqrt{(n+1)(N_b - N_a + n + 1)}\end{aligned} \tag{24}$$

with $n = [0, N_a - 1]$, and

$$\begin{aligned}(M)_{N_a+1-n,N_a+1-n} &= \langle N_a - n|_{\mathrm{B}}\langle n|_{\mathrm{A}} H^{\mathrm{eff}}|n\rangle_{\mathrm{A}}|N_a - n\rangle_{\mathrm{B}} \\ &= N_a U\end{aligned} \tag{25}$$

with $n = [0, N_a]$. It is obviously an $(N_a + 1)$ -order Jordan block, satisfying

$$\begin{aligned}[(M - N_a UI)^{N_a}]_{ij} = \prod_{n=0}^{N_a-1} \frac{4\kappa^2}{U}\frac{N_a - n}{N_b} \\ \times \sqrt{(n+1)(N_b - N_a + n + 1)}\delta_{N_a+1,1}.\end{aligned} \tag{26}$$

where I is the unit matrix. In other words, matrix $(M - N_a UI)$ is a nilpotent matrix, i.e.,

$$(M - N_a UI)^{N_a+1} = 0. \tag{27}$$

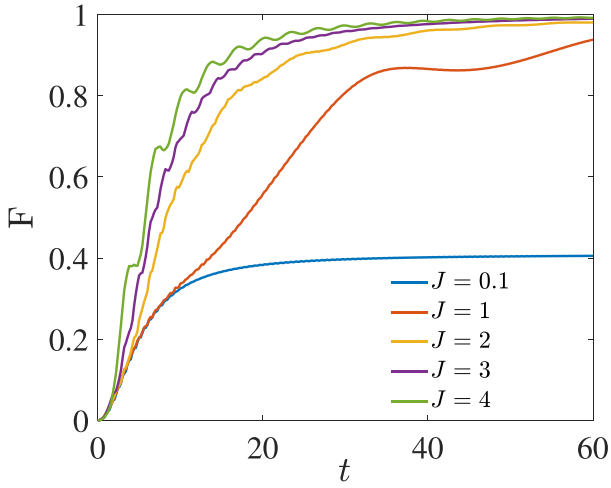

FIG. 3. The plot of $F(t)$, which is obtained by exact diagonalization of the original Hamiltonian for the finite system. The parameters are $N_a = 2$, $N_b = 4$, $\kappa = 1$, $U = 20$, $J_{ij} = J$. Several typical values of J are taken and indicated in the panels.

Taking $N_a = N_b = 4$, for example, the matrix has the form

$$M = \frac{2\kappa^2}{U}\begin{pmatrix} 0 & 0 & 0 & 0 & 0 \\ 2 & 0 & 0 & 0 & 0 \\ 0 & 3 & 0 & 0 & 0 \\ 0 & 0 & 3 & 0 & 0 \\ 0 & 0 & 0 & 2 & 0 \end{pmatrix} + 4UI, \tag{28}$$

which possesses a single eigenvector $(0 \quad 0 \quad 0 \quad 0 \quad 1)^T$.

The dynamics for any states in this subspace is governed by the time evolution operator

$$U(t) = e^{-iMt} = e^{-iN_aUt}\sum_{l=0}^{N_a}\frac{1}{l!}[-i(M - N_aUI)t]^l. \tag{29}$$

It indicates that for the initial state $|\Psi(0)\rangle = |A\rangle$, we have

$$\begin{aligned} |\Psi(t)\rangle &= e^{-iMt}|A\rangle \\ &= e^{-iN_aUt}(1 \quad f_1 \quad \ldots \quad f_q \quad \ldots \quad f_{N_a})^T, \end{aligned} \tag{30}$$

where the elements

$$f_q = \sqrt{A^q_{N_a}A^q_{N_b}}\left(\frac{-4i\kappa^2 t}{UN_b}\right)^q, \quad q \in [1, N_a] \tag{31}$$

$$A^q_{N_a} = \frac{N_a!}{(N_a - q)!}, \quad A^q_{N_b} = \frac{N_b!}{(N_b - q)!}, \tag{32}$$

and

$$||\Psi(t)\rangle| = \sqrt{1 + \sum_{q=1}^{N_a}|f_q|^2} \approx |f_{N_a}| \tag{33}$$

at large $t \gg \frac{UN_b}{\kappa^2}$. Setting the target state as

$$|\Psi_{\text{target}}\rangle = |B\rangle, \tag{34}$$

we have the fidelity

$$F(t) = \frac{|\langle\Psi_{\text{target}}|\Psi(t)\rangle|}{||\Psi(t)\rangle|} = \frac{|f_{N_a}|}{||\Psi(t)\rangle|} \approx 1, \tag{35}$$

which indicates that state $|\Psi_{\text{target}}\rangle$ becomes dominant in the evolved state $|\Psi(t)\rangle$ at large $t \gg \frac{UN_b}{\kappa^2}$. The increasing behavior of $||\Psi(t)\rangle|$ obeying $||\Psi(t)\rangle|^2 \propto t^{2N_a}$ within the large t region is also a dynamic demonstration for the order of the Jordan block. This analytical analysis shows that the speed of relaxation of the ODLRO pair state depends on the order of the EP, which is determined by the number of pairs. Furthermore, we would like to address two points. (i) The non-Hermitian effective Hamiltonian $H^{\text{eff}}_{\text{AB}}$ is obtained from the simplest case with $N_a = N_b = 1$ in Appendix A. Its validity for large systems is illustrated in Appendix B for the large U limit and from the perspective of parameters approaching the EP. (ii) The power behavior of $||\Psi(t)\rangle|$ requires large t. However, in practice, $F(t)$ may approach unity before this time domain.

V. DYNAMIC TRANSITION

The above analysis provides a prediction about the dynamic transition from an insulating state to an η-pairing state in a composite non-Hermitian system. The composite system consists of two parts (or two layers): one is a trivial system (source system) constructed by a set of isolated sites, while the other is a Hubbard model (central system), which supports η-pairing eigenstates. Initially, two subsystems are separated and the source system is fully filled by electrons, being in an insulating state, while the central system is empty. The decoupling between two subsystems can be achieved in two ways, i.e., the prequench Hamiltonian can be set by (a) taking the chemical potential on a source system far from the resonant energy of the central system; and (b) switching off the tunneling terms between two subsystems directly under the resonant condition. The postquench Hamiltonian is then $H_{\text{A}} + H_{\text{B}} + H_{\text{AB}}$. According to our analysis, both quench dynamics should result in a steady superconducting state, realizing the dynamic transition from an insulating state to an η-pairing state.

We perform numerical simulations on a finite system with the following considerations. (i) The analysis based on the effective Hamiltonian in last section only predicts the results for large U within a large time domain. The efficiency of the scheme should be estimated from numerical simulations of the original Hamiltonian. (ii) The existence of η-pairing eigenstates is independent of the distribution of the hoppings for B sublattices. The evolved states $|\Psi(t)\rangle$ for initial states $|2\rangle_{\text{A}}|0\rangle_{\text{B}}$ and $|3\rangle_{\text{A}}|0\rangle_{\text{B}}$ in two finite systems are computed by exact diagonalization. We focus on the Dirac probability

$$P(t) = ||\Psi(t)\rangle|^2, \tag{36}$$

and the fidelity

$$F(t) = \frac{1}{\sqrt{P}}|\langle\Psi_{\text{target}}|\Psi(t)\rangle|, \tag{37}$$

with the target states being $|0\rangle_{\text{A}}|2\rangle_{\text{B}}$ and $|0\rangle_{\text{A}}|3\rangle_{\text{B}}$, respectively. The lattice geometry and numerical results are plotted in Fig. 2. We plot the fidelity as a function of U for three

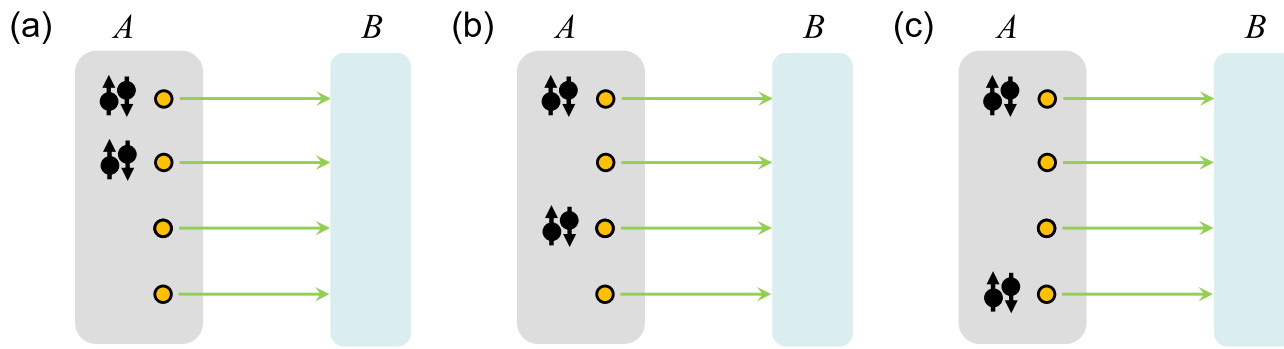

FIG. 4. Schematics of the composite non-Hermitian system with different initial states. (a), (b), and (c) present three typical configurations, in which two doublons are located in different sites of system A. The analytical analysis based on the perturbation method in large U limit indicates that the final states after a long time are the same. Numerical simulations for finite U and a small-size system support this conclusion.

typical instants. We find that there exists an optimal $U \approx 5$, at which the fidelity gets the maximal value. We also plot the probability $\ln P(t)$ as a function of $\ln t$ to demonstrate the EP dynamic behavior. From the results of linear fitting, it can be seen that the slope of the line deviates from the predicted value for the cases with small U, especially for larger systems. This indicates that the speed of relaxation of the pair state depends on the order of the EP and the fidelity of the scheme is immune to the irregularity of the lattice. We estimated the relation of the hopping strength and the efficiency of the scheme from numerical simulations of the original Hamiltonian in Fig. 3. Within a certain range of parameters, the increase of the hopping strength will improve the efficiency of the scheme.

VI. SUMMARY AND DISCUSSION

In summary, we have extended the scheme of quantum casting to interacting many-body systems. Unlike the previous work Ref. [20] on noninteracting systems, the present scheme does not require the scan on the chemical potential of the source system. Our findings offer a method for the efficient preparation of correlated states and are expected to be necessary and insightful for quantum engineering. The key point is the exceptional dynamics, which allows particles pumping from the source subsystem to the central subsystem, realizing the dynamical preparation of many-body quantum states. It is due to the resonance between the initial state and the target state. Accordingly, there is a class of initial states (see Fig. 4) evolving to the same final state after a long time. Numerical simulations for finite U and a small-size system support this conclusion. In this sense, such a scheme can be applied to other interacting many-body systems. On the other hand, considering a quench process with the prequench Hamiltonian being $H_A + H_B$, and the postquench Hamiltonian being $H_A + H_B + H_{AB}$, the Loschmidt echo $|L|^2 = |\langle\Psi(0)|\Psi(t)\rangle|^2$ should turn to zero after a long time for a finite system. It may predict an *asymptotic* dynamic quantum phase transition (DQPT) [19] in thermodynamic limit, i.e., $|L|^2$ decays rapidly, rather than vanishes at a finite instant in a standard DQPT. The final answer depends on the scaling behavior of $|L|^2$, which is an open question at the present stage.

ACKNOWLEDGMENT

This work was supported by National Natural Science Foundation of China (under Grant No. 11874225).

APPENDIX A

In this Appendix, we present a derivation of the effective Hamiltonian in the doublon subspace for the tunneling term between two subsystems A and B. We will obtain the effective Hamiltonian from the time evolution operator rather than the perturbation method due to the concern with the availability of it for a non-Hermitian system at exceptional point.

Consider a two-site Hamiltonian

$$H_{\text{conn}} = \sum_{\sigma=\uparrow,\downarrow} \kappa b_\sigma^\dagger a_\sigma + U b_\uparrow^\dagger b_\downarrow^\dagger b_\downarrow b_\uparrow + \frac{U}{2}(a_\uparrow^\dagger a_\uparrow + a_\downarrow^\dagger a_\downarrow), \tag{A1}$$

which describes the connection between any two sites among A and B subsystems. We neglect the subscripts of the operators for the sake of simplicity. We start from the matrix representation of the Hamiltonian in the invariant subspace spanned by the basis set

$$\begin{aligned} |1\rangle &= |\uparrow\downarrow\rangle_A|0\rangle_B = a_\uparrow^\dagger a_\downarrow^\dagger|\text{Vac}\rangle, \\ |2\rangle &= |0\rangle_A|\uparrow\downarrow\rangle_B = b_\uparrow^\dagger b_\downarrow^\dagger|\text{Vac}\rangle, \\ |3\rangle &= |\uparrow\rangle_A|\downarrow\rangle_B = a_\uparrow^\dagger b_\downarrow^\dagger|\text{Vac}\rangle, \\ |4\rangle &= |\downarrow\rangle_A|\uparrow\rangle_B = a_\downarrow^\dagger b_\uparrow^\dagger|\text{Vac}\rangle \end{aligned} \tag{A2}$$

which is

$$h = \begin{pmatrix} U & 0 & 0 & 0 \\ 0 & U & \kappa & -\kappa \\ \kappa & 0 & \frac{U}{2} & 0 \\ -\kappa & 0 & 0 & \frac{U}{2} \end{pmatrix}, \tag{A3}$$

which contains a 2×2 Jordan block for nonzero U. The solution of the matrix consists of three eigenvectors $|\phi_c\rangle$, $|\phi_3\rangle$, and $|\phi_4\rangle$, with eigenvalues U, $U/2$, and $U/2$, respectively. The

explicit form of the vectors is

$$|\phi_a\rangle = \begin{pmatrix} 1 \\ 0 \\ \frac{2\kappa}{U} \\ -\frac{2\kappa}{U} \end{pmatrix}, \quad |\phi_c\rangle = \begin{pmatrix} 0 \\ 1 \\ 0 \\ 0 \end{pmatrix},$$
$$|\phi_3\rangle = \begin{pmatrix} 0 \\ -\frac{2\kappa}{U} \\ 1 \\ 0 \end{pmatrix}, \quad |\phi_4\rangle = \begin{pmatrix} 0 \\ \frac{2\kappa}{U} \\ 0 \\ 1 \end{pmatrix}, \tag{A4}$$

where $|\phi_c\rangle$ is the coalescing vector and $|\phi_a\rangle$ is the corresponding auxiliary vector, satisfying

$$(h - UI)|\phi_a\rangle = |\phi_c\rangle, \tag{A5}$$

where I is the unit matrix. We would like to point out that in the case of $U = 0$, h contains a 3×3 Jordan block. The solution of the matrix consists of two eigenvectors $|\phi_c\rangle$ and $|\phi_4\rangle$, with the same eigenvalue 0. The explicit form of the vectors is

$$|\phi_a\rangle = \begin{pmatrix} 1 \\ 0 \\ 0 \\ 0 \end{pmatrix}, \quad |\phi_c\rangle = \begin{pmatrix} 0 \\ 1 \\ 0 \\ 0 \end{pmatrix}, \quad |\phi_4\rangle = \begin{pmatrix} 0 \\ 0 \\ 1 \\ 1 \end{pmatrix}, \tag{A6}$$

where $|\phi_c\rangle$ is the coalescing vector and $|\phi_a\rangle$ is the corresponding auxiliary vector. In this work, we only focus on the case with nonzero U. However, one should consider the effect of three-order EP when U is very small. Then the time evolution operator in such a invariant subspace can be obtained as

$$e^{-iht} = e^{-itU} \begin{pmatrix} 1 & 0 & 0 & 0 \\ -\frac{4it\kappa^2}{U} - \frac{8\kappa^2}{U^2}\Lambda & 1 & \frac{2\kappa}{U}\Lambda & -\frac{2\kappa}{U}\Lambda \\ \frac{2\kappa}{U}\Lambda & 0 & e^{\frac{itU}{2}} & 0 \\ -\frac{2\kappa}{U}\Lambda & 0 & 0 & e^{\frac{itU}{2}} \end{pmatrix}, \tag{A7}$$

where $\Lambda = 1 - e^{itU/2}$. The time evolution of the trivial initial state $|\phi_a\rangle$ can be expressed as

$$|\Psi(t)\rangle = e^{-iht}|\phi_a\rangle = e^{-itU} \begin{pmatrix} 1 \\ -\frac{4it\kappa^2}{U} - \frac{8\kappa^2}{U^2}\Lambda \\ \frac{2\kappa}{U} \\ -\frac{2\kappa}{U} \end{pmatrix}. \tag{A8}$$

We find that

$$\langle 2|\Psi(t)\rangle = -e^{-itU}\frac{4\kappa^2}{U}\left[it + \frac{2}{U}(1 - e^{itU/2})\right], \tag{A9}$$

which can be valued within finite time scale as

$$\langle 2|\Psi(t)\rangle \approx -e^{-itU}\frac{4\kappa^2}{U}\begin{cases} it, & \text{large } U \\ \frac{U}{4}t^2, & \text{small } U. \end{cases} \tag{A10}$$

Note that the switching of powers of the variable t is due to the cancellation of the linear t term in the small U limit. It is in accordance with the above analysis about the order of the Jordan block. In the large U limit, $U \gg \kappa$, e^{-iht} reduces to a diagonal-block form

$$e^{-iht} \approx e^{-itU} \begin{pmatrix} 1 & 0 & 0 & 0 \\ -\frac{4it\kappa^2}{U} & 1 & 0 & 0 \\ 0 & 0 & e^{itU/2} & 0 \\ 0 & 0 & 0 & e^{itU/2} \end{pmatrix}. \tag{A11}$$

Then in the doublon subspace spanned by $a^\dagger_\uparrow a^\dagger_\downarrow|\text{Vac}\rangle$ and $b^\dagger_\uparrow b^\dagger_\downarrow|\text{Vac}\rangle$, the effective Hamiltonian is

$$H^{\text{eff}}_{\text{conn}} = \frac{4\kappa^2}{U} b^\dagger_\uparrow b^\dagger_\downarrow a_\downarrow a_\uparrow + UI_2. \tag{A12}$$

APPENDIX B

In this Appendix, we obtain the effective Hamiltonian of the tunneling term H_{AB} with arbitrary size for the large U limit from the perspective of parameters approaching the EP. At first, we add a unidirectional tunneling term $\lambda a^\dagger_{l,\sigma} b_{l,\sigma}$ and take the parameter κ_{ij} as a constant $\kappa\delta_{ij}$ for simplicity. The new tunneling between the two subsystems H_{A} and H_{B} reads

$$H'_{\text{AB}} = \sum_{\sigma=\uparrow,\downarrow}\sum_l (\kappa b^\dagger_{l,\sigma} a_{l,\sigma} + \lambda a^\dagger_{l,\sigma} b_{l,\sigma}). \tag{B1}$$

We introduce a set of canonical operators

$$\bar{c}_{l,\sigma} = \sqrt{\frac{\lambda}{\kappa}} a^\dagger_{l,\sigma}, \qquad c_{l,\sigma} = \sqrt{\frac{\kappa}{\lambda}} a_{l,\sigma},$$
$$\bar{d}_{l,\sigma} = b^\dagger_{l,\sigma}, \qquad d_{l,\sigma} = b_{l,\sigma}, \tag{B2}$$

which obey the commutative relations

$$\{c_{l,\sigma}, \bar{c}_{l',\sigma'}\} = \delta_{ll'}\delta_{\sigma\sigma'}, \quad \{\bar{c}_{l,\sigma}, \bar{c}_{l',\sigma'}\} = \{c_{l,\sigma}, c_{l',\sigma'}\} = 0,$$
$$\{d_{l,\sigma}, \bar{d}_{l',\sigma'}\} = \delta_{ll'}\delta_{\sigma\sigma'}, \quad \{\bar{d}_{l,\sigma}, \bar{d}_{l',\sigma'}\} = \{d_{l,\sigma}, d_{l',\sigma'}\} = 0. \tag{B3}$$

The transformation in Eq. (B2) is essentially a similarity transformation with singularities at $\lambda = 0$ and $\kappa = 0$, beyond which it allows us to rewrite the Hamiltonian in the form

$$H'_{\text{AB}} = \sum_{\sigma=\uparrow,\downarrow}\sum_l [\sqrt{\lambda\kappa}\bar{d}_{l,\sigma} c_{l,\sigma} + \sqrt{\lambda\kappa}\bar{c}_{l,\sigma} d_{l,\sigma}]. \tag{B4}$$

So far, H'_{AB} has become a Hermitian Hamiltonian, which allows us to employ the perturbation method to get the effective Hamiltonian

$$(H'_{\text{AB}})^{\text{eff}} = -\frac{8}{U}\sum_l \Big(-\frac{\kappa^2\eta^-_{\text{A},l}\eta^+_{\text{B},l}}{2} - \frac{\lambda^2\eta^+_{\text{A},l}\eta^-_{\text{B},l}}{2} + \lambda\kappa\eta^z_{\text{A},l}\eta^z_{\text{B},l} - \frac{\lambda\kappa}{4}\Big). \tag{B5}$$

Although the above solution is only true for nonzero λ, one can extrapolate the approximate solution at $\lambda = 0$ by taking $\lambda \to 0$. In the limit of zero λ, we have $H'_{\text{AB}} \to H_{\text{AB}}$ and $(H'_{\text{AB}})^{\text{eff}} \to H^{\text{eff}}_{\text{AB}}$.

[1] J. Hubbard, Electron correlations in narrow energy bands, Proc. R. Soc. A **276**, 238 (1963).

[2] S. Jochim, M. Bartenstein, A. Altmeyer, G. Hendl, S. Riedl, C. Chin, J. Hecker Denschlag, and R. Grimm,

Bose-Einstein condensation of molecules, Science **302**, 2101 (2003).
[3] M. Greiner, C. A. Regal, and D. S. Jin, Emergence of a molecular Bose–Einstein condensate from a Fermi gas, Nature (London) **426**, 537 (2003).
[4] M. P. A. Fisher, P. B. Weichman, G. Grinstein, and D. S. Fisher, Boson localization and the superfluid-insulator transition, Phys. Rev. B **40**, 546 (1989).
[5] A. Georges, G. Kotliar, W. Krauth, and M. J. Rozenberg, Dynamical mean-field theory of strongly correlated fermion systems and the limit of infinite dimensions, Rev. Mod. Phys. **68**, 13 (1996).
[6] B. Keimer, S. A. Kivelson, M. R. Norman, S. Uchida, and J. Zaanen, From quantum matter to high-temperature superconductivity in copper oxides, Nature (London) **518**, 179 (2015).
[7] P. A. Lee, N. Nagaosa, and X.-G. Wen, Doping a Mott insulator: Physics of high-temperature superconductivity, Rev. Mod. Phys. **78**, 17 (2006).
[8] C. N. Yang, η Pairing and Off-Diagonal Long-Range Order in a Hubbard Model, Phys. Rev. Lett. **63**, 2144 (1989).
[9] S. Choi, J. Choi, R. Landig, G. Kucsko, H. Zhou, J. Isoya, F. Jelezko, S. Onoda, H. Sumiya, V. Khemani, C. v. Keyserlingk, N. Y. Yao, E. Demler, and M. D. Lukin, Observation of discrete time-crystalline order in a disordered dipolar many-body system, Nature (London) **543**, 221 (2017).
[10] D. V. Else, B. Bauer, and C. Nayak, Floquet Time Crystals, Phys. Rev. Lett. **117**, 090402 (2016).
[11] V. Khemani, A. Lazarides, R. Moessner, and S. L. Sondhi, Phase Structure of Driven Quantum Systems, Phys. Rev. Lett. **116**, 250401 (2016).
[12] N. H. Lindner, G. Refael, and V. Galitski, Floquet topological insulator in semiconductor quantum wells, Nat. Phys. **7**, 490 (2011).
[13] T. Kaneko, T. Shirakawa, S. Sorella, and S. Yunoki, Photoinduced η Pairing in the Hubbard Model, Phys. Rev. Lett. **122**, 077002 (2019).
[14] J. Tindall, B. Buča, J. R. Coulthard, and D. Jaksch, Heating-Induced Long-Range η Pairing in the Hubbard Model, Phys. Rev. Lett. **123**, 030603 (2019).
[15] X. Z. Zhang and Z. Song, η-pairing ground states in the non-Hermitian Hubbard model, Phys. Rev. B **103**, 235153 (2021).
[16] X. M. Yang and Z. Song, Resonant generation of a p-wave Cooper pair in a non-Hermitian Kitaev chain at the exceptional point, Phys. Rev. A **102**, 022219 (2020).
[17] M. Rigol, V. Dunjko, and M. Olshanii, Thermalization and its mechanism for generic isolated quantum systems, Nature (London) **452**, 854 (2008).
[18] J. Eisert, M. Friesdorf, and C. Gogolin, Quantum many-body systems out of equilibrium, Nat. Phys. **11**, 124 (2015).
[19] M. Heyl, Dynamical quantum phase transitions: A brief survey, Europhys. Lett. **125**, 26001 (2019).
[20] X. M. Yang and Z. Song, Quantum mold casting for topological insulating and edge states, Phys. Rev. B **103**, 094307 (2021).
[21] M. V. Berry, Physics of nonhermitian degeneracies, Czech. J. Phys. **54**, 1039 (2004).
[22] W. D. Heiss, The physics of exceptional points, J. Phys. A: Math. Theor. **45**, 444016 (2012).
[23] M.-A. Miri and A. Alú, Exceptional points in optics and photonics, Science **363**, eaar7709 (2019).
[24] X. Zhang and J. Gong, Non-Hermitian Floquet topological phases: Exceptional points, coalescent edge modes, and the skin effect, Phys. Rev. B **101**, 045415 (2020).
[25] L. Jin, P. Wang, and Z. Song, Su-Schrieffer-Heeger chain with one pair of $\mathcal{PT}$-symmetric defects, Sci. Rep. **7**, 5903 (2017).
[26] P. Wang, K. L. Zhang, and Z. Song, Transition from degeneracy to coalescence: Theorem and applications, Phys. Rev. B **104**, 245406 (2021).
[27] T. Kato, *Perturbation Theory of Linear Operator* (Springer, Berlin, 1966).
[28] M. Müller and I. Rotter, Exceptional points in open quantum systems, J. Phys. A: Math. Theor. **41**, 244018 (2008).
[29] N. Moiseyev, *Non-Hermitian Quantum Mechanics* (Cambridge University Press, Cambridge, UK, 2011).
[30] E. J. Bergholtz, J. Carl Budich, and F. K. Kunst, Exceptional topology of non-Hermitian systems, Rev. Mod. Phys. **93**, 015005 (2021).
[31] J. Doppler, A. A. Mailybaev, J. Böhm, U. Kuhl, A. Girschik, F. Libisch, T. J. Milburn, P. Rabl, N. Moiseyev, and S. Rotter, Dynamically encircling an exceptional point for asymmetric mode switching, Nature (London) **537**, 76 (2016).
[32] H. Xu, D. Mason, L. Jiang, and J. G. E. Harris, Topological energy transfer in an optomechanical system with exceptional points, Nature (London) **537**, 80 (2016).
[33] S. Assawaworrarit, X. Yu, and S. Fan, Robust wireless power transfer using a nonlinear parity–time-symmetric circuit, Nature (London) **546**, 387 (2017).
[34] J. Wiersig, Enhancing the Sensitivity of Frequency and Energy Splitting Detection by Using Exceptional Points: Application to Microcavity Sensors for Single-Particle Detection, Phys. Rev. Lett. **112**, 203901 (2014).
[35] J. Wiersig, Sensors operating at exceptional points: General theory, Phys. Rev. A **93**, 033809 (2016).
[36] H. Hodaei, A. U. Hassan, S. Wittek, H. Garcia-Gracia, R. El-Ganainy, D. N. Christodoulides, and M. Khajavikhan, Enhanced sensitivity at higher-order exceptional points, Nature (London) **548**, 187 (2017).
[37] W. Chen, Ş. Kaya Özdemir, G. Zhao, J. Wiersig, and L. Yang, Exceptional points enhance sensing in an optical microcavity, Nature (London) **548**, 192 (2017).
[38] K. Ding, G. Ma, M. Xiao, Z. Q. Zhang, and C. T. Chan, Emergence, Coalescence, and Topological Properties of Multiple Exceptional Points and Their Experimental Realization, Phys. Rev. X **6**, 021007 (2016).
[39] Y.-X. Xiao, Z.-Q. Zhang, Z. H. Hang, and C. T. Chan, Anisotropic exceptional points of arbitrary order, Phys. Rev. B **99**, 241403(R) (2019).
[40] L. Pan, S. Chen, and X. Cui, Interacting non-Hermitian ultracold atoms in a harmonic trap: Two-body exact solution and a high-order exceptional point, Phys. Rev. A **99**, 063616 (2019).